EXAMINING TROPICAL CYCLONE RAINBANDS AS DETECTED BY GROUND- AND SPACE-BASED RADARS

Corene J. Matyas[1] *, Zainab S. Ali[1], Kimberly M. Wood[2], Stephanie E. Zick[3]

[1]University of Florida, Gainesville, Florida; [2]Mississippi State University, Starkville, Mississippi; [3]Virginia Tech, Blacksburg, Virginia

1. INTRODUCTION

The Weather Surveillance Radar 1988-Doppler (WSR-88D) network (Crum et al. 1993) detects precipitation events at high spatial and temporal resolution. Beam spreading and arcing limits their use at far distances from a site and thus the network features ~150 radars placed so that the radar beams overlap to help in detecting synoptic-scale weather systems as they move across the country. As each radar is operated indepedently, there are differences in scanning strategy, signal strength, amount of beam spreading, and timing of scans that can cause the same place in the atmosphere to have different reflectivity values (Gourley et al. 2003).

The rainbands of Tropical cyclones (TCs) contain a mix of stratiform and convective clouds (Jorgensen 1984) that produce high rain rates. They frequently cause flooding as they move over land (Elsberry 2002) where scans from the WSR-88D network can reveal the rainband structures and identify regions producing high rain rates that could lead to flooding. However, TCs spend most of their existence over the ocean and out of range of ground-based radars. To better understand the evolution of TC rainband structures over their entire lifecycles, they need to be detected by radars that are not located on land.

The Dual-frequency Precipitation Radar (DPR) (Le and Chandrasekar 2013) from the Global Precipitation Measurement (GPM) observatory provides an opportunity to detect weather systems from a top-down perspective whether over land or ocean. These scans can provide important details about the structure of TC rainbands (Hence and Houze 2012) and how the storm is evolving when the storm is out of WSR-88D range as well as provide a comparable measurement for locations sampled by multiple WSR-88D beams (Li et al. 2020). In this case study, we examine differences between DPR reflectivity and four WSR datasets: point-matched WSR-88D values in space and time (Keem et al. 2019), the Multi-Radar/Multi-Sensor System quality-controlled reflectivity mosaic (Zhang et al. 2016), and mosaics we created (Tang and Matyas 2016) using time-distance weight and retaining the maximum value, for two differently-structured TCs.

* Corresponding author address:
Corene J. Matyas, Univ. of Florida, Dept. of Geography, Gainesville, FL 32611-7315; e-mail matyas@ufl.edu

2. DATA

In this case study, we examine data from GPM overpasses for Tropical Storm Isaias and Hurricane Laura. The GPM overpass for Isaias occurred at 04 Aug 2020 0852 UTC. Isaias made landfall as a Category 1 hurricane nine hours earlier over North Carolina. At overpass time, its maximum sustained winds were 60 kt and it was undergoing a transition to become an extratropial cyclone. It was declared post tropical at 00 UTC on 05 August. The DPR passed directly over the TC center and also sampled a long swatch over its outer rainbands that stretched along a stationary front northeast of center.

Hurricane Laura's overpass occurred at 27 Aug 2020 0300 UTC. Laura was at its maximum intensity with winds of 130 kt, a Category 4 hurricane and was three hours prior to landfall over Louisiana.The DPR did not sample the entire eyewall of Laura as the trajectory of the GPM satellite was to the left of the TC center.

We obtained reflectivity from the DPR V07A from Nasa's website (URL). The values are available ~5 km irregular grid over a 245 km-wide swath with a range resolution of 250 m, and there is a minimum value of 14 dBZ.

We also obtained volume- matched data for ground-based radars (GR) from the NASA for GPM ground validation (https://gpm-gv.gsfc.nasa.gov/). Reflectivity data were obtained from five radars, two that sampled Laura (KLCH and KPOE), and three than sampled Isaias (KAKQ, KDOX, KRAX). In addition to the reflectivity values from the DPR and ground radar (GR), we also analyze data on the altitude, precipitation type (stratiform, convective, or a mixed-type), and bright band altitude if available. More details on this type of analysis are available in Keem et al. (2019).

To compare these precisely-matched data points from a volumetric analysis with gridded reflectivity datasets along a constant altitude, we examine data from MRMS and two of our own mosaics. For MRMS comparison, we used quality-controlled reflectivity which are available every two minutes at a 0.01° latitude x 0.01° longitude x 1 km altitude resolution. We selected the time closest to DPR overpass as we cannot location precise information on what the timestamp of the MRMS data signifies.

We also create our own mosaic of WSR data utilizing two different approaches. Our code first analyzes data at each radar that is within 750 km of a TC's center. Stations are analyzed on individual grids with spacing of 1 km x 1 km x 500 m. The radar antenna is placed at the 0, 0, 0 coordinate. The scan closest to the GPM overpass is ingested, converted into cartesian coordinates, and values at each gate populate the grid. When multiple values are available for a grid cell, we employ two methods to determine the final value. Firstly, we use a time-distance weight (TDW) so that the value from the closest radar and nearest the desired output time is given the highest weight when the values are averaged (Zhang et al. 2005). Secondly, we retain the maximum value (MAX) in that grid cell. Empty grid cells are then filled using a nearest-neighbor scheme. Each of these strategies was employed separately. We then save a constant altitude slice for 2, 3, and 4 km to match the availability of MRMS data. We do not analyze data at 5 km or higher due to the presence of the brightband as given in the volume-matched dataset.

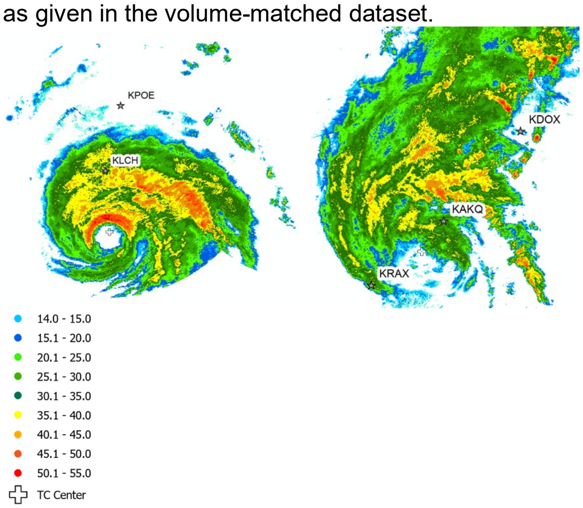

Fig. 1. Mosaics using all available radars and Max strategy for a) Laura and b) Isaias. Locations of five radars with point-matched data available are shown.

3. METHODS

We employ a Geographic Information System (GIS) to match the values from the mosaicked datasets to the coordinates from the DPR and GR data. We utilize the extract values to points tool which takes the value from the grid cell that form which each data point falls. As the gridded datasets are constant-altitude slices, we only utilize data from the DPR and GR datasets that are within 250 m of 2, 3, or 4 km. Given that the DPR has a minimum of 14 dBZ, we remove datapoints from consideration if values from any of the datasets are below 14 dBZ or are missing for that coordinate. Given that the "other" precipitation type is only present in <1% of points, we also eliminate these points. While we retain the reflectivity values from each dataset (Figs. 2 and 3), we also subtract each GR-based value from DPR (Figs. 4 and 5).

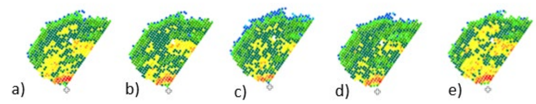

Fig. 2. Reflectivity values for Laura a) DPR, b) GR, c) MRMS, d) TDW, e) MAX.

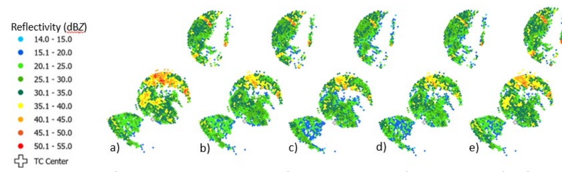

Fig. 3. Reflectivity values for Isaias a) DPR, b) GR, c) MRMS, d) TDW, e) MAX.

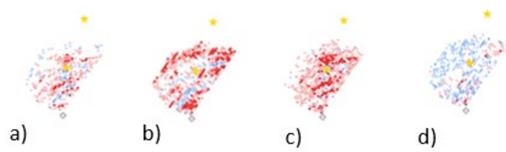

Fig. 4: Reflectivity difference a) DPR-GR, b) DPR-MRMS, c) DPR-TDW, d) DPR-MAX.

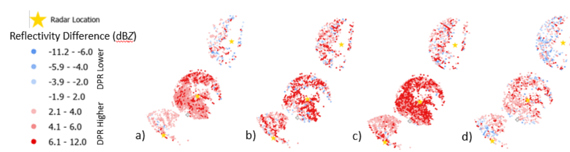

Fig. 5: Reflectivity difference a) DPR-GR, b) DPR-MRMS, c) DPR-TDW, d) DPR-MAX.

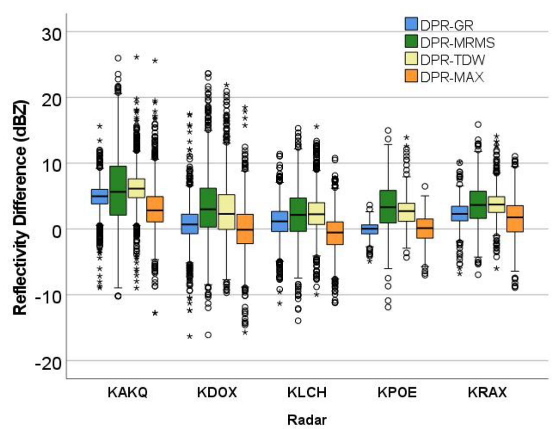

Fig. 6. Box plot showing mean, 25 and 75th %, and outliers for reflectivity differences for each radar.

We perform two kinds of statistical tests. On the reflectivity values, we perform paired-sample t tests where the null hypothesis is that means from the two populations are equal. We set α = 0.05 and run ten tests for each radar as there are 5 reflectivity values for each radar and each pair is tested (e.g., DPR vs GR, DPR vs MRMS, DPR vs MAX).

For the reflectivity difference, we employ nonparametric independent samples tests on difference values by mosaic altitude (3 groups – Kruskal Wallis test), and precipitation type (2 groups – Mann-Whitney *U* test). The null hypothesis is that the distribution of samples is the same across groups and α = 0.05.

4. RESULTS

4.1 Paired-Sample T Tests

Of the 50 paired-sample t tests performed, 42 tests showed data had significantly different means. Being that DPR and GR are volume-matched, we hypothesized that these two datasets would produce the most similar results. Yet of the eight cases where similar means occurred, only one was between DPR and GR (Table 1). At radar KPOE which sampled the outer edge of Hurricane Laura and did not sample the eyewall, values were similar between DPR, GR, and MAX. That the one instance of DP and GR having similar means also occurs when DPR and MAX have similar means suggests that employing a weighting scheme might be lowering the values.

The pair that was similar with the most frequency was MRMS and TDW. Values were similar at four of the five radars examined. With average reflectivity about 3 dBZ lower, MRMS and TDW produced similar results at KPOE. The fact that our TDW mosaic produced results similar to MRMS helps to validate our weighted mosaic methodology. In that DPR and MAX were similar at two of the radars suggests that retaining the maximum value is an approach that more closely approaches that of DPR over the TDW or MRMS weighted methods. These tests help to confirm what can be seen visually in Figures 2 and 3, that higher values are present for images a and e compared to b, c, and d. When reflectivity values are subtracted, we can see that there is a strong low bias for MRMS and TDW (Figures 4bc and 5bc, while values are higher in MAX than DPR (Figures 4d and 5d). We can also see that results vary by radar as the largest low bias occurs for KAKQ.

Plotting the data on boxplots allows the spread of values to be visualized (Fig. 6). DPR-GR tends to have the lowest spread between the 25-75th percentiles while DPR-MRMS has the highest. The spread and average values also differ among the radars. Difference values are the highest on average at KAKQ while this location and KDOX display a relatively large number of outliers.

Table 1: Results with p > 0.01 from paired-sample T tests for reflectivity.

Radar	N	Data 1	Data 1 Mean (dB*Z*)	Data 2	Data 2 Mean (dB*Z*)	t	*p* Value
KAKQ	1472	MRMS	29.19	TDW	28.90	2.202	0.028
KDOX	965	DPR	29.96	MAX	29.99	-0.242	0.809
KRAX	591	MRMS	22.88	TDW	22.77	0.567	0.571
KLCH	1480	MRMS	30.54	TDW	30.28	2.258	0.024
KPOE	305	DPR	27.75	GR	27.85	-1.508	0.133
KPOE	305	DPR	27.75	MAX	27.88	-0.636	0.525
KPOE	305	GR	27.85	MAX	27.88	0.148	0.883
KPOE	305	MRMS	24.50	TDW	25.01	-1.843	0.066

4.2 Independent Samples Tests

We first compared results by altitude (Table 2) with a hypothesis that the lower altitudes could be a closer match as the WSR beam is more horizontal. Altitude did not make a difference for the weighted mosaics. Results for DPR-GR show that the best match occurred at 2 km and worst at 3 km although the value at 4 km was very close to 3 km. The result is right at the p value for rejecting the null hypothesis. The test statistic is very high for DPR-MAX and the difference values improve with height. The boxplots (Fig. 7) show the improvement of DPR-MAX with height and show that fewer outliers occurred at the 4 km altitude compared to 2 or 3 km.

Table 2. Results from Kruskal Wallis tests for reflectivity difference by mosaic altitude.

Difference	Altitude (km)	N	Mean	Std. Dev.	Test Statistic	p Value
DPR-GR	2	2067	2.14	2.98	5.988	0.050
	3	1556	2.33	3.10		
	4	1180	2.27	3.35		
DPR-MRMS	2	2067	3.92	5.12	0.699	0.705
	3	1556	3.80	4.98		
	4	1180	3.83	4.75		
DPR-TDW	2	2067	3.94	3.86	0.923	0.630
	3	1556	3.93	3.66		
	4	1180	3.78	3.76		
DPR-MAX	2	2067	1.85	3.92	254.302	<0.001
	3	1556	0.43	3.47		
	4	1180	-0.07	3.15		

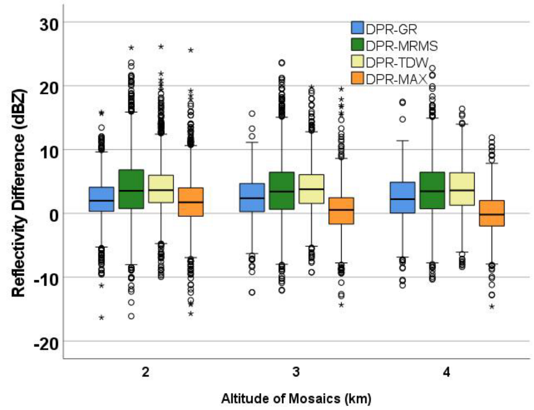

Fig. 7. As in Fig. 6 for altitude of mosaic.

We next compared results by precipitation type. We hypothesized that stratiform could have lower differences that convective given how vertically-oriented convective clouds are and with the time offsets for the WSR scans, the convective clouds might have shifted on the grid between the times of the DPR and WSR scans.In this case, it should be a consistent result across all of the datasets as all WSR data were from the same timestamp. Our hypothesis is confirmed (Table 3) as the four comparisons feature a more close association between DPR and WSR in stratiform precipitation than in convective precipitation. Differences in the sample means varied from ~0.6 in the volume-matchup to nearly 1 dBZ in our two mosaics. However, the values were lowest for DPR-MAX indicating a better match-up overall. Fig. 8 shows that although the differences were lower overall for DPR-MAX, outliers were fewer for DPR-GR. This could be attributed to DPR-GR being a precise altitude match whereas DPR-GR are matched through a 500 m range of altitudes. We can also see that the standard deviation is highest for DPR-MRMS and it is higher for convective than stratiform precipitation.

Table 3. Results from Kruskal Wallis tests for reflectivity difference by precipitation type.

Difference	**Precip. Type**	**N**	**Mean (dBZ)**	**Std. Deviation**	**t**	**Two-Sided *p* Value**
DPR-GR	Stratiform	4122	2.15	2.95	-3.84	<0.01
	Convective	681	2.75	3.90		
DPR-MRMS	Stratiform	4122	3.77	4.82	-2.55	0.01
	Convective	681	4.38	5.87		
DPR-TDW	Stratiform	4122	3.76	3.62	-5.18	<0.01
	Convective	681	4.71	4.53		
DPR-MAX	Stratiform	4122	0.79	3.53	-5.2	<0.01
	Convective	681	1.72	4.48		

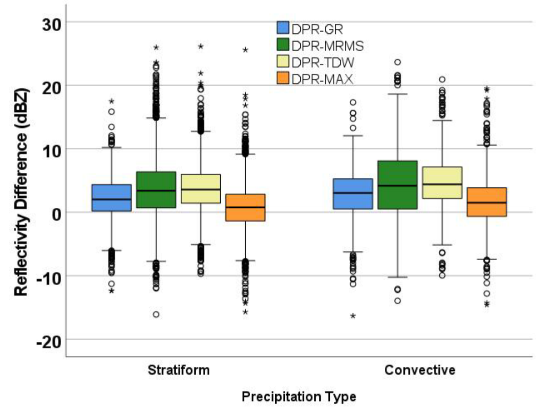

Fig. 8. As in Fig. 6 for type of precipitation.

5. CONCLUSIONS

Overall, MAX values were closer to DPR than the other 3 datasets although many points had higher values than DPR. The best match between DPR and MAX occurred at 4 km although the difference at 3 km averaged less that 0.5 dBZ. Values were closer in stratiform than convective precipitation. Although it was true for all comparisons. One limitatino of the MAX approach is that sharp gradients are introduced and the impact of this might account for the larger standard deviation in the DPR-MAX results compared to the DPR-GR results. That difference in standard deviation could also be caused by the 500 m altitude range in the DPR-MAX points compared to a more precise altitude match in the DPR-GR dataset.

Whether point-matched without interpolation, or interpolated to a regular grid, ground-based reflectivity values vary in their relationship to DPR. Each radar site also exhibited a differencnt range of reflectivity values. Differences by radar could be due to running hot or cold, detecting different parts of the storm and amounts of the storm's edge where a sharp gradient in reflectivity occurs, and/or sweep time relative to DPR overpass. For example, The volume scan for KAKQ started six minutes before the DPR overpass, giving the storm's edge and small regions of convective precipitation time to move both tangentially and along the storm's path between the two scans. Future research should examine regions where WSR scans overlap to better define differences due to running hor or cold and timing of the scane relative to the DPR overpass.

6. ACKNOWLEDGEMENTS

This research was funded the National Science Foundation AGS-2012008

7. REFERENCES

Crum, T. D., R. L. Alberty, and D. W. Burgess, 1993: Recording, archiving, and using WSR-88D data. *Bull. Amer. Meteor. Soc.*, **74,** 645-653.

Elsberry, R. L., 2002: Predicting hurricane landfall precipitation: Optimistic and pessimistic views from the symposium on precipitation extremes. *Bull. Amer. Meteor. Soc.*, **83,** 1333-1339.

Gourley, J., B. Kaney, and R. Maddox, 2003: Evaluating the calibrations of radars: A software approach. *Preprints, 31st Int. Conf. on Radar Meteorology, Seattle, WA, Amer. Meteor. Soc*, 462.

Hence, D. A., and R. A. Houze, 2012: Vertical structure of tropical cyclone rainbands as seen by the TRMM precipitation radar. *J. Atmos. Sci.*, **69,** 2644-2661.

Jorgensen, D. P., 1984: Mesoscale and convective-scale characteristics of mature hurricanes. Part I: General observations by research aircraft. *J. Atmos. Sci.*, **41,** 1268-1285.

Keem, M., B.-C. Seo, W. F. Krajewski, and K. R. Morris, 2019: Inter-comparison of reflectivity measurements between GPM DPR and NEXRAD radars. *Atmos. Res.*, **226,** 49-65.

Le, M., and V. Chandrasekar, 2013: Precipitation Type Classification Method for Dual-Frequency Precipitation Radar (DPR) Onboard the GPM. *IEEE Trans. Geosci. Remote Sensing*, **51,** 1784-1790.

Li, Z., and Coauthors, 2020: Cross-Examination of Similarity, Difference and Deficiency of Gauge, Radar and Satellite Precipitation Measuring Uncertainties for Extreme Events Using Conventional Metrics and Multiplicative Triple Collocation. *Remote Sensing*, **12,** 1258.

Tang, J., and C. J. Matyas, 2016: Fast playback framework for analysis of ground-based Doppler radar observations using Map-Reduce technology. *J. Atmos. Ocean. Technol.*, **33,** 621-634.

Zhang, J., K. Howard, and J. Gourley, 2005: Constructing three-dimensional multiple-radar reflectivity mosaics: Examples of convective storms and stratiform rain echoes. *J. Atmos. Ocean. Technol.*, **22,** 30-42.

Zhang, J., and Coauthors, 2016: Multi-Radar Multi-Sensor (MRMS) quantitative precipitation estimation: Initial operating capabilities. *Bull. Amer. Meteor. Soc.*, **97,** 621-638.